Temperature response of luminescent tris(bipyridine)ruthenium(II)-doped silica nanoparticles

Martín Mirenda, Valeria Levi, Mariano Luis Bossi, Luciana Bruno, Andrea V. Bordoni, Alberto E. Regazzoni, Alejandro Wolosiuk

PII: S0021-9797(12)01105-8
DOI: http://dx.doi.org/10.1016/j.jcis.2012.09.059
Reference: YJCIS 18264

To appear in: *Journal of Colloid and Interface Science*

Please cite this article as: M. Mirenda, V. Levi, M.L. Bossi, L. Bruno, A.V. Bordoni, A.E. Regazzoni, A. Wolosiuk, Temperature response of luminescent tris(bipyridine)ruthenium(II)-doped silica nanoparticles, *Journal of Colloid and Interface Science* (2012), doi: http://dx.doi.org/10.1016/j.jcis.2012.09.059

Temperature response of luminescent tris(bipyridine)ruthenium(II)-doped silica nanoparticles

Martín Mirenda,[1,2] Valeria Levi,[3] Mariano Luis Bossi,[2] Luciana Bruno,[4] Andrea V. Bordoni,[1] Alberto E. Regazzoni[1,*] and Alejandro Wolosiuk[1,*]

[1] Gerencia Química, Centro Atómico Constituyentes, Comisión Nacional de Energía Atómica. Av. Gral. Paz 1499, B1650KNA, San Martín, Buenos Aires, Argentina.

[2] Departamento de Química Inorgánica, Analítica y Química Física, Facultad de Ciencias Exactas y Naturales, Universidad de Buenos Aires. Ciudad Universitaria, Pab. II. C1428EHA, Buenos Aires, Argentina.

[3] Laboratorio de Dinámica Intracelular, Departamento de Química Biológica, Facultad de Ciencias Exactas y Naturales, Universidad de Buenos Aires. Ciudad Universitaria, Pab. II. C1428EHA, Buenos Aires, Argentina.

[4] Grupo de Dinámica y Transporte Intracelular, Departamento de Física, Facultad de Ciencias Exactas y Naturales, Universidad de Buenos Aires. Ciudad Universitaria, Pab. I. C1428EHA, Buenos Aires, Argentina.

* Corresponding author:

Alberto E. Regazzoni
phone: + (54-11) 6772-7179
fax: + (54-11) 6772-7886
e-mail: regazzon@cnea.gov.ar

Alejandro Wolosiuk
phone: + (54-11) 6772-7947
fax: + (54-11) 6772-7886
e-mail: wolosiuk@cnea.gov.ar

Abstract

Nanoparticle-based temperature imaging is an emerging field of advanced applications. Herein, the sensitivity of the phosphorescence of tris(bipyridine)ruthenium(II)-doped silica nanoparticles towards temperature is studied. 130 nm size particles were prepared by a modification of Stöber's method, that allows the incorporation of $Ru[(bpy)_3]^{2+}$ into the outer particle shell. The entrapped $Ru[(bpy)_3]^{2+}$ retains its photophysical properties, yet the emission of the particles is not affected by the presence of O_2, neither by anionic quenchers; quenching by MV^{2+}, on the other hand, is strongly dependent on pH. Between 20 and 60 ºC, the steady-state emission of the particles decreases linearly with increasing temperature. The slope of the straight line diminishes slightly on thermal cycling, but soon stabilizes. Fluorescence measurements by scanning confocal microscopy indicate that the silica nanoparticles doped with $Ru[(bpy)_3]^{2+}$ can indeed be employed to probe thermal processes in micro-environments.

Keywords: fluorescent nanoparticles; doped silica; tris(bipyridine)ruthenium(II); luminescent temperature nanosensors; fluorescence quenching

Introduction

The development of temperature sensors at the micro- and nanoscale has recently received considerable attention due to the growing interest to perform measurements on a variety of unconventional systems, e.g., cells [1,2], lab-on-chip and microfluidic devices [3-5]. The different approaches for the design of thermometers at the nanoscale have been reviewed by Lee and Kotov [6]. Among the different nanomaterials, emitting ones appear to have attractive advantages due to the high sensibility that can be achieved by fluorescence detection [7]; furthermore, they offer the possibility of imaging and mapping [4,8]. Luminescent thermometry relies on the change of the fluorescence or phosphorescence of photoactive materials that is produced by the temperature dependence of radiative and non-radiative transition rates.

One appealing strategy resorts to the encapsulation of fluorescent dyes into appropriate colloidal matrixes [8], including SiO_2. Dye-doped SiO_2 nanoparticles are ideal for bioanalytical applications because they are chemically inert and are not subjected to microbial attack. In addition, silica surfaces can be easily tailored [9,10]. Incorporation of rhodamine 6G, acridine orange and $[Ru(bpy)_3]^{2+}$ into growing SiO_2 particles has already been described in the literature [11-15]. Despite the emission spectra of the aqueous $[Ru(bpy)_3]^{2+}$ complex, which has a large Stokes fluorescent shift, and decreases linearly with increasing temperature [4], the ability of tris(bipyridine)ruthenium(II)-doped silica nanoparticles ($Ru(bpy)_3@SiO_2$ NPs) to sense temperature changes has not yet been reported.

Here, aiming at assessing the actual potential of this system, we describe the synthesis of silica nanoparticles doped with tris(bipyridine)ruthenium(II), and explore their photophysical properties in an attempt to contribute to the development of thermo-responsive colloids.

Experimental Section

Materials

Tetraethoxysilane (TEOS, Sigma-Aldrich), tris(bipyridine)ruthenium(II) chloride ($Ru(bpy)_3Cl_2$, Sigma-Aldrich), absolute ethanol (Merck), polyethyleneimine (PEI, MW 50-60 kDa, 50% w/w solution, Aldrich), methylviologen dichloride hydrate ($MVCl_2$, Aldrich, 98% purity), potassium hexacyanoferrate(II) trihydrate ($K_4Fe(CN)_6.3H_2O$, Sigma-Aldrich, 99% purity), HCl (Merck), KCl (Merck) and NaOH (Merck) were used as received. Deionized water (18 MΩ cm^{-1}) was obtained from Milli-Q system.

Synthesis

$Ru(bpy)_3@SiO_2$ NPs were prepared as sketched in Fig. 1. First, SiO_2 cores were synthesized following the procedure proposed by Stöber [16], which is based on the reaction of TEOS, NH_3 and H_2O in EtOH. After keeping the system at 40ºC for two hours, 0.6 mg $Ru(bpy)_3Cl_2$ dissolved in 0.5 mL EtOH and 300 µL neat TEOS were added simultaneously to the reaction mixture. The suspension was then left overnight under mild stirring. Particles were washed repeatedly with EtOH and H_2O, and finally kept as an aqueous dispersion. No dissolved $[Ru(bpy)_3]^{2+}$ could be detected after the synthesis.

Characterization

Particle size was assessed by field emission-scanning electron microscopy (FE-SEM), and dynamic light scattering (DLS) measurements. FE-SEM images were taken with a Zeiss Leo 982 Gemini microscope in the secondary-electron mode using an in-lens detector. DLS measurements were carried out in a Brookhaven BI-200 SM apparatus fitted with an avalanche photodiode detector and a He-Ne laser (wavelength 637 nm).

ζ-potential measurements were performed in a Malvern Zetasizer 2000 instrument. For this purpose, particles were appropriately diluted in 10 mM KCl solutions of given pH values; pH was adjusted by adding HCl or KOH, and measured using a Metrohm 654 pH-meter and a combined glass-electrode.

Steady-state fluorescence spectra were recorded using a Felix X32 PTI fluorometer, equipped with a xenon short-arc lamp UXL-75XE, and a thermostated sample-holder. The excitation wavelength (λ_{exc}) was 463 nm, and the emitted light was collected at 90º with respect to the excitation beam. To study the influence of MV^{2+} and $Fe(CN)_6^{4-}$ on the particles fluorescence, a given volume of 0.04 % w/w aqueous suspension of $Ru(bpy)_3@SiO_2$ NPs of fixed pH was placed in a 1 × 1 cm quartz cell, and the emission (I_0) recorded. Then, a measured amount of the quencher was added to the cuvette, and the emission (I) read after 5 minutes equilibration under magnetic stirring; prior the reading, pH was readjusted, if necessary. I values were corrected for dilution. All measurements were carried out under ambient oxygen, unless stated otherwise. When required, O_2 was scrubbed by bubbling O_2-free nitrogen through the suspension.

The anisotropy of the steady-state emission was determined in the usual manner [17]. Since the total light collected by the detector is composed by the scattered excitation light and the emitted one, $<r>_{Total}$ need to be corrected to discard the former contribution. This is made by expressing $<r>_{Total}$ in terms of the additive law of anisotropies (Eq. 1), assessing the fractions of light due to scattering (x_{Sc}) and $Ru(bpy)_3@SiO_2$ fluorescence (x_F) directly from the emission spectrum, and determining $<r>_{Sc}$ from a separate experiment performed using 130 nm silica NPs.

$$< r >_{Total} = x_{Sc} < r >_{Sc} + x_F < r >_F \quad (1)$$

Scanning confocal microscopy (SCM) images were obtained using an Olympus FV-1000 microscope. The excitation source was a solid diode laser at 458 nm (average power at the sample, 10 μW). The laser light was reflected by a dichroic mirror (DM458/515) and focused on the sample by means of an Olympus UPlanSApo 60x oil immersion objective (NA = 1.35). The fluorescence of the $Ru(bpy)_3@SiO_2$ NPs was collected by the same objective, passed through a pinhole, reflected on a diffraction grating, passed through a slit, set to

transmit in the 550 – 650 nm range, and detected by a photon-counting photomultiplier. The temperature of the sample was controlled using a Solent Scientific environmental chamber. Image analyses were performed using the ImageJ® software. The *z*-confocal resolution is ca. 600 nm, whereas lateral one, limited by optical diffraction, is in the order of 200 to 300 nm.

The inspected specimens were prepared by electrostatic self-assembly [18], as follows: 22 × 22 mm thoroughly-cleaned glass slides were successively immersed in a 1% w/w PEI solution for 10 min, and in a dilute dispersion of colloidal $Ru(bpy)_3@SiO_2$ for 1 min, and rinsed finally with water to remove any possible excess of particles.

The fluorescence of $Ru(bpy)_3@SiO_2$ NPs was assessed by analyzing SCM images. To do so, the position coordinates of the center of a given isolated nanoparticle (x_i,y_i) was first determined, by eye inspection, from images taken in the transmission mode. Then, a 10×10 pixels region of interest (ROI) centered at x_i,y_i is defined in the confocal image; this procedure of centering the ROI avoids bias due to intensity threshold criteria or eye inspection of SCM images. Afterwards, two intensity profiles are built in the *x*- and *y*-directions; this was done by averaging the intensity of 1×3 (or 3×1) pixels spots. The profiles were then fitted to a Gaussian function and their amplitudes compared; if they differ in more than 50%, the point was discarded from the analysis. This procedure was repeated in 70 different spots of each image, from which ca. 50 fluorescence intensity values were obtained. Profile fittings were carried out using computation routines written and ran in the MATLAB® environment; computationally, this procedure is much less expensive than 2D Gaussian fitting.

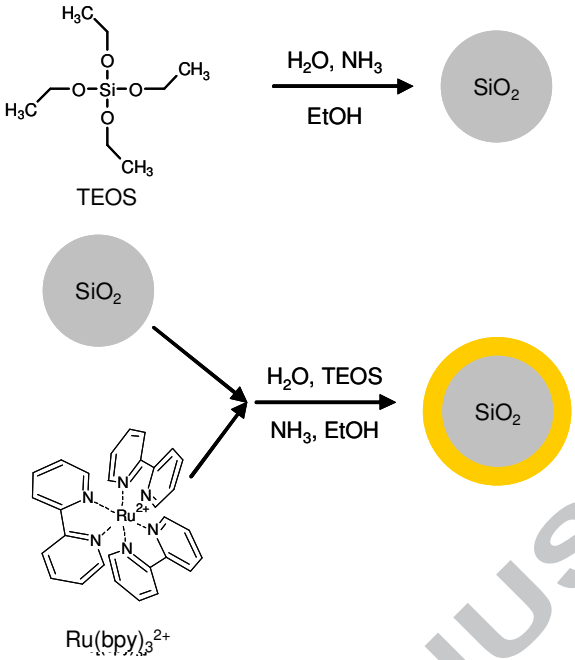

Fig. 1. Sketch representation of the steps involved in the synthesis of $Ru(bpy)_3@SiO_2$ NPs.

Results and Discussion

Uniform spherical $Ru(bpy)_3@SiO_2$ nanoparticles were produced in a two-steps procedure that is an adaptation of the well-known Stöber's method [16] and follows the ideas introduced by Matijević and co-workers [11]. In the first step (Fig. 1), monodispersed SiO_2 seeds are formed, the size of which can be adjusted by appropriate setting of the synthesis parameters. In the second one, the cores are covered by a thin silica shell, which during growth entraps the fluorophore, aided by the electrostatic attraction between $[Ru(bpy)_3]^{2+}$ and negatively charged silica oligomers. This approach allows reducing the concentration of the dye used during the synthesis, hence minimizing the increase of ionic strength that would affect particle stability [19]. Fig. 2a shows an FE-SEM image of the so-synthesized $Ru(bpy)_3@SiO_2$ NPs. They are very uniform spheres of 130 nm diameter. Their narrow size distribution was further confirmed by DLS measurements (Fig. 2b), which yielded a somewhat larger mean radius. The noted difference is in line with the fact that DLS measures

hydrodynamic diameters, but it may also reflect swelling of the dispersed Stöber's spheres [20].

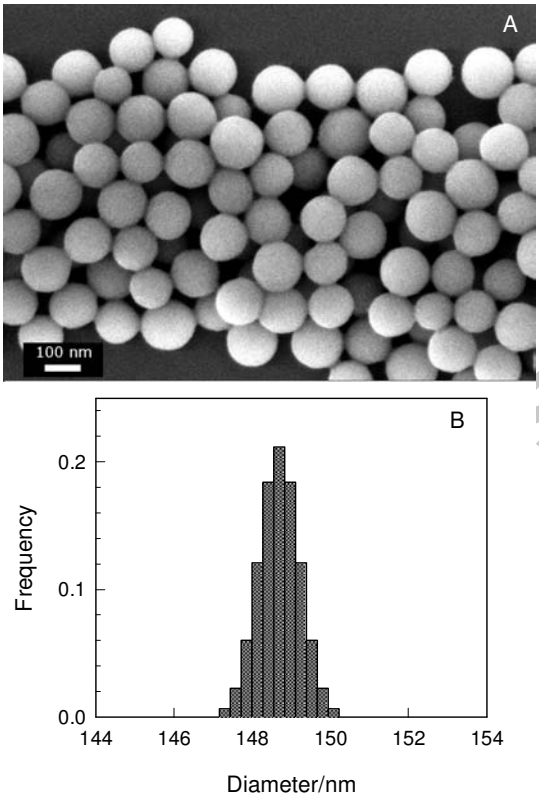

Fig. 2. FE-SEM micrograph (A) and hydrodynamic size distribution (B) of $Ru(bpy)_3@SiO_2$ NPs.

The visible spectrum of aqueous $[Ru(bpy)_3]^{2+}$ is characterized by an absorption band centered at 450 nm due to the Ru(4d)-bpy(π^*) transition to the ^{1}MLCT state (MLCT, metal-to-ligand charge transfer). This state evolves in an intersystem crossing of unitary quantum yield to the ^{3}MLCT triplet that decays via radiative and non-radiative pathways [21,22]. The steady-state emission spectrum of $Ru(bpy)_3@SiO_2$ NPs dispersed in water is shown in Fig. 3. Maximum phosphorescence is detected at 595 nm. The band is blue-shifted with respect to that of free aqueous $[Ru(bpy)_3]^{2+}$, which is observed at 610 nm [23]. This shift, which is characteristic of "rigidochromism" [24-27], indicates that the complex has indeed been entrapped into the SiO_2 matrix during the formation of the shell. Furthermore, the measured

steady-state emission anisotropy of the $Ru(bpy)_3@SiO_2$ NPs dispersions is 0.11 ± 0.01 (see Supplementary data), very close to that of $[Ru(bpy)_3]^{2+}$ immobilized in rigid glasses [28-30]; on the other hand, the emission of the aqueous complex is totally depolarized, thus <r> = 0.

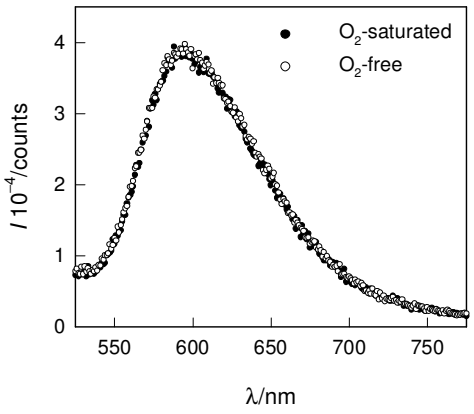

Fig. 3. Emission spectra of $Ru(bpy)_3@SiO_2$ NPs dispersed in O_2-free and O_2-saturated water; λ_{exc} = 463 nm; slit = 0.5 mm.

The emission of dissolved $[Ru(bpy)_3]^{2+}$ is highly dependent on O_2 concentration. Whilst such sensitivity is actually the basis of many oxygen sensors [31], it may be detrimental for other applications. Fig. 3 compares the emission of $Ru(bpy)_3@SiO_2$ dispersed in O_2-free and O_2-saturated aqueous solutions. Interestingly, dissolved oxygen has a null effect on the steady-state emission of the immobilized complex (Fig. 3). A similar effect has already been observed for encapsulated $[Ru(phen)_3]^{2+}$, a fact that was attributed to the low oxygen permeability of the silica shell [12,13]. Whether the SiO_2 framework hinders the diffusion of O_2 in such a significant manner remains an open question.

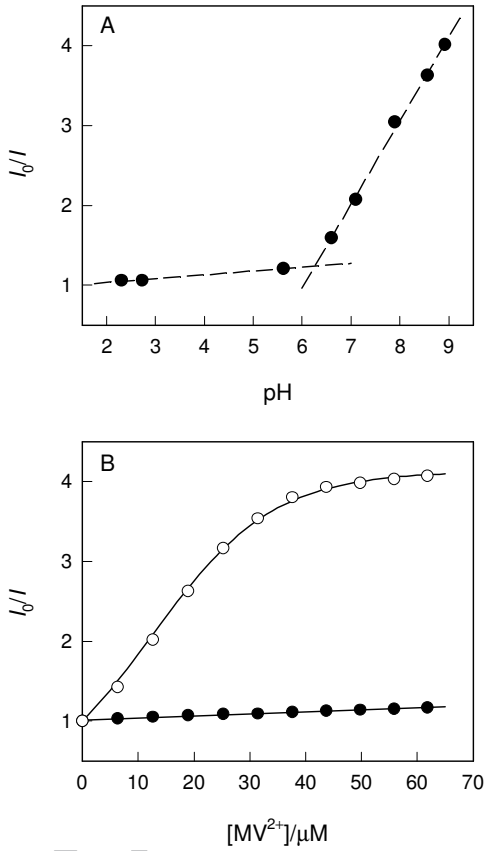

Fig. 4. Quenching of the emission at 595 nm of $Ru(bpy)_3@SiO_2$ NPs by MV^{2+} as a function of pH (A) and MV^{2+} concentration (B); in A, $[MV^{2+}]$ = 62 μM; in B, pH 3.0 (●), pH 8.9 (○).

Stöber SiO_2 particles are by no means impenetrable spheres [32]. They have a rather open framework that allows the transport of ions [33,34]. Incidentally, the porous double layer model was proposed to account for the notably high uptake of counterions at SiO_2/water interfaces [35,36]. Therefore it is likely that small ionic quenchers, such as, MV^{2+} or $Fe(CN)_6^{4-}$, may affect the luminescence of the excited $Ru(bpy)_3@SiO_2$ NPs; both ions are efficient electron acceptors, with homogeneous quenching rate constants in the order of 10^9 L mol^{-1} s^{-1} [23]. The quenching of the steady-state fluorescence by $Fe(CN)_6^{4-}$ is negligible, even at rather high $Fe(CN)_6^{4-}$ concentrations (see Supplementary data), and independent of pH. On the contrary, quenching by MV^{2+} is notable and strongly dependent of pH (Fig. 4). At

low pH values, the ratio I_0/I increases slowly with pH (Fig. 4a). However, once pH surpasses the isoelectric point (iep) of the $Ru(bpy)_3@SiO_2$ NPs, which is ca. 4.0 (see Supplementary data), the slope rises markedly. Since in solution the quenching of the fluorescence of $[Ru(bpy)_3]^{2+}$ by MV^{2+}, or $Fe(CN)_6^{4-}$, is independent of pH, the observed trend must be attributed to the electrostatic nature of the sorption of the quenchers, which, depending of their charge, permeate the gel-like shell of the particles.

The shape of the concentration dependence of the quenching is also a function of pH (Fig. 4b). Below the iep, I_0/I increases linearly and very modestly with $[MV^{2+}]$, whereas at pH 8.9 the decrease of the steady-state fluorescence is initially much steeper and tends to level-off at the higher methyl viologen concentrations. Despite the latter profile is not really langmuirian, the simplest explanation traces the observed trends to quencher sorption; the adsorption equilibrium constant of MV^{2+} on SiO_2 nanoparticles at pH 10 has been reported to be 4.7×10^5 M^{-1} [37]. It is possible that the Stern-Volmer relationship casted in terms of the surface excess of the quencher would not suffice to account for the shape of the I_0/I vs $[MV^{2+}]$ plots, and that the influence of other factors, such as the size of the active sphere of quenching, may need to be considered. Notably, there is a significant fraction of entrapped $[Ru(bpy)_3]^{2+}$ that cannot be accessed by the quencher, and 25 % of the initial fluorescence remains at the higher MV^{2+} concentrations.

The insensitivity of the steady-state fluorescence of $Ru(bpy)_3@SiO_2$ NPs towards ubiquitous oxygen, negatively charged quenchers, and the important fraction of $[Ru(bpy)_3]^{2+}$ that is inaccessible to positive ones, make them suitable for field assays or analysis on complex samples, including live (biological) tests. One possible application is temperature sensing. As already mention, the excited ^{3}MLCT state of $[Ru(bpy)_3]^{2+}$ decays via parallel pathways. The non-radiative one, which involves intersystem crossing to the ^{3}*d-d* state, is thermally activated. As a consequence, the phosphorescence of the free aqueous complex

decreases with increasing temperature [4]. Fig. 5 shows that $Ru(bpy)_3@SiO_2$ NPs behave in the same manner. More important, however, is the fact that the decrease of the intensity of the emission peak is linear ($r^2 = 0.996$) in the range $20 \leq T/^oC \leq 60$ (Fig. 5b), a temperature range of relevance for biological systems. Due to the activated nature of the intersystem crossing, linearity outside these limits is not warranted.

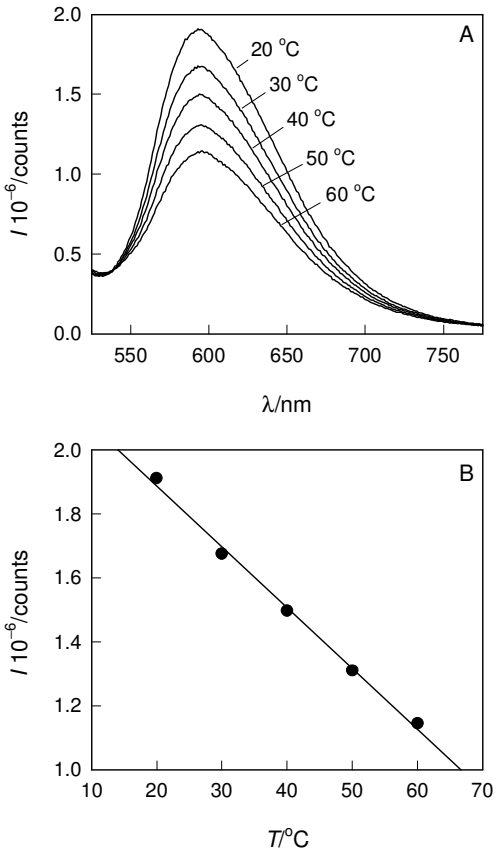

Fig. 5. Emission spectra of $Ru(bpy)_3@SiO_2$ NPs (A), and emission at 595 nm (B) as a function of temperature; λ_{exc} = 463 nm; slit = 1.6 mm.

The emission of the dispersed $Ru(bpy)_3@SiO_2$ NPs, however, decreases upon cycling the temperature between 20 and 60 °C (Fig. 6, inset); the slopes of the *I* vs *T* straight lines also decrease (Fig. 6). The effect of temperature cycles cannot be attributed to leaching of the complex, as no dissolved $[Ru(bpy)_3]^{2+}$ could be detected. The origin of the observed decays is

not obvious. One possible explanation invokes maturation of colloidal SiO_2, as subjecting the system to high temperatures should induce further cross-linking within the particles, which, in turn, may affect the photophysical properties of the entrapped complex. In fact, the emission quantum yield of $[Ru(phen)_3]^{2+}$ was found to decrease two-fold upon incorporation into SiO_2 particles [13]. Nonetheless, whatever the source of the decrease in the emission, Fig. 6 shows that both steady-state fluorescence and d*I*/d*T* values become stable after seven cycles without any significant loss in sensitivity. This indicates that $Ru(bpy)_3@SiO_2$ NPs, once properly conditioned, can actually be used to sense temperature changes; data presented in Fig. 5 correspond to the 9th cycle.

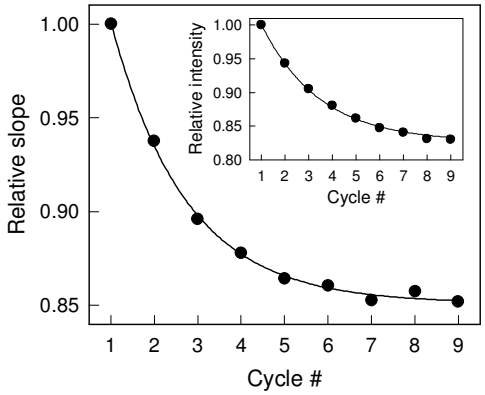

Fig. 6. Temperature response of the emission of $Ru(bpy)_3@SiO_2$ NPs after thermal cycling. The inset shows the decay of the maximum emission.

To explore the ability of the $Ru(bpy)_3@SiO_2$ NPs to sense temperature changes in microenvironments, thermally stabilized $Ru(bpy)_3@SiO_2$ NPs assembled onto a PEI-modified glass slide were scrutinized under a scanning confocal microscope. SCM images taken at different temperatures are presented in Fig. 7a. Importantly, the mean fluorescence intensity decreases linearly with increasing temperature (Fig. 7b).

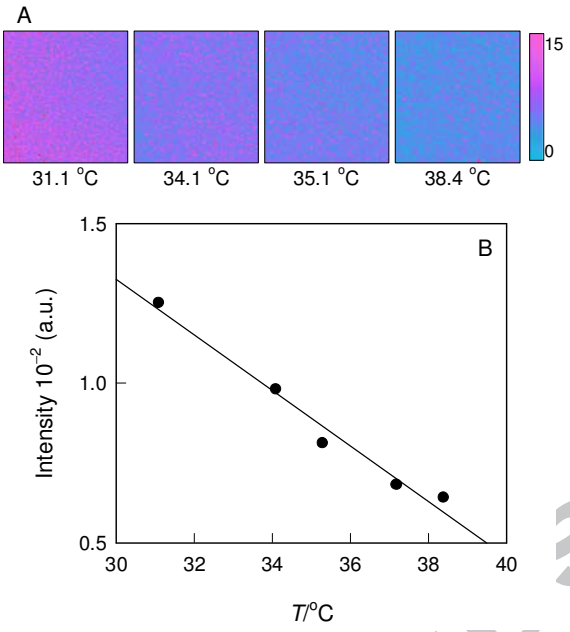

Fig. 7. 20 × 20 μm SCM images of $Ru(bpy)_3@SiO_2$ NPs adhered to PEI-modified glass (A), and mean fluorescence intensity as a function of temperature (B).

Confocal microscopy offers, in addition, the possibility of probing the fluorescence of individual nanoparticles, despite their size is below the spatial resolution of the microscope. For this purpose, the location (*x*,*y* coordinates) of the center of each isolated nanoparticle was determined from images taken in the transmission mode (Fig. 8a). Then, the coordinates were positioned in the confocal images (Fig. 8b), from which the average intensity of 1×3 (or 3×1) pixels spots were measured along the *x* and *y* directions. Typical profiles, which correspond to the same nanoparticle at two different temperatures, are shown in Fig. 8c. Fig. 8d further shows that the width of the distribution of the mean fluorescence of the nanoparticles is nearly insensitive to temperature changes. Overall, Fig. 8 illustrates that the emission of individual $Ru(bpy)_3@SiO_2$ NPs follows the expected temperature trend, and that the modified Stöber particles can indeed be employed to sense thermal processes in confined environments.

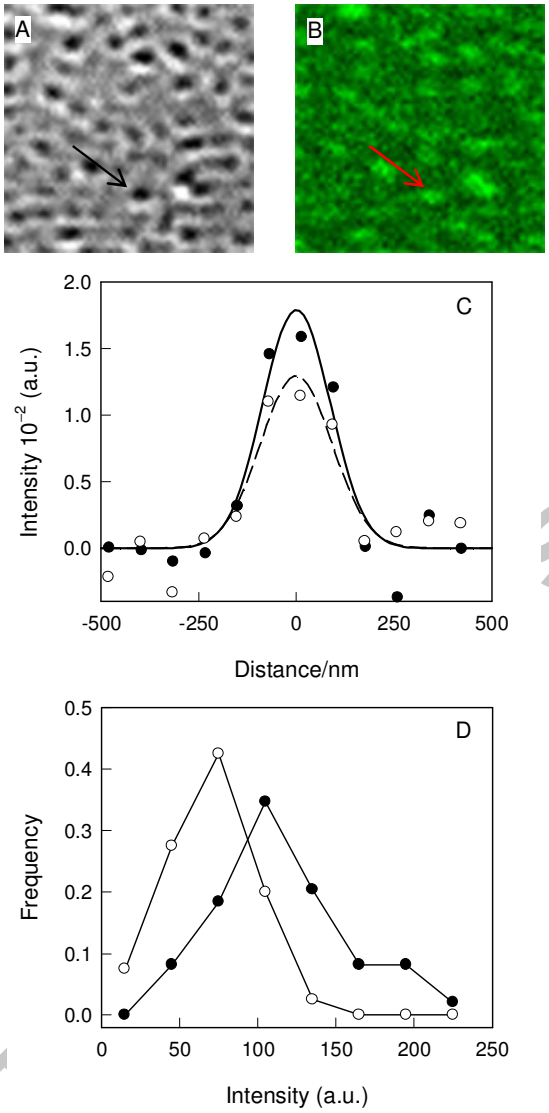

Fig. 8. 10 × 10 μm light transmission (A) and SCM (B) images of $Ru(bpy)_3$@SiO_2 NPs adhered to PEI-modified glass. (C) Intensity profiles of the spot marked with the arrow in A and B at 31.1 °C (●) and 38.4 °C (○); thick lines are Gaussian fits. (D) Particle fluorescence histogram for 31.1 °C (●) and 38.4 °C (○).

Conclusions

This study demonstrates that tris(bipyridine)ruthenium(II)-doped silica nanoparticles retain the photophysical properties of the free complex, and that the temperature dependence of their fluorescence can be exploited to develop thermo-sensing devices in the micrometric scale. Their insensitivity towards ubiquitous oxygen and anionic quenchers make them

suitable to probe microenvironments of different nature, including biological ones; due care, however, ought to be taken to minimize the effect of cationic quenchers.

Acknowledgements

V.L., L.B., M.L.B., A.E.R. and A.W. are members of CONICET. M.M. and A.V.B. are thankful to CONICET for granting a post-doctoral fellowship. Financing was provided by CONICET PIP 11220090101031, ANPCyT (PICT 2008-1104), UBACyT (20020090200201) and Gabbos. L.B. acknowledges Dr. S. Kristel for moral support.

References

[1] F. Vetrone, R. Naccache, A. Zamarrón, A.J. De La Fuente, F. Sanz-Rodríguez, L.M. Maestro, E.M. Rodriguez, D. Jaque, J.G. Sole, J.A. Capobianco, ACS Nano 4 (2010) 3254-3258.

[2] J.M. Yang, H. Yang, L. Lin, ACS Nano 5 (2011) 5067-5071.

[3] D. Ross, M. Gaitan, L.E. Locascio, Anal. Chem. 73 (2001) 4117-4123.

[4] O. Filevich, R. Etchenique, Anal. Chem. 78 (2006) 7499-7503.

[5] L.H. Thamdrup, N.B. Larsen, A. Kristensen, Nano Lett. 10 (2010) 826-832.

[6] J. Lee, N.A. Kotov, Nano Today 2 (2007) 48-51.

[7] S. Wang, S. Westcott, W. Chen, J. Phys. Chem. B 106 (2002) 11203-11209.

[8] X.D. Wang, X.H. Song, C.Y. He, C.J. Yang, G. Chen, X. Chen, Anal. Chem. 83 (2011) 2434-2437.

[9] M. Arduini, S. Marcuz, M. Montolli, E. Rampazzo, F. Mancin, S. Gross, L. Armelao, P. Tecilla, U. Tonellato, Langmuir 21 (2005) 9314-9321.

[10] F. Caruso, Colloids and colloid assemblies. Wiley-VCH Weinheim, 2004.

[11] M. Bele, O. Siiman, E. Matijević, J. Colloid Interface Sci. 254 (2002) 274-282.

[12] D. Zhang, Z. Wu, J. Xu, J. Liang, J. Li, W. Yang, Langmuir 26 (2010) 6657-6662.

[13] L.M. Rossi, L. Shi, F.H. Quina, Z. Rosenzweig, Langmuir 21 (2005) 4277-4280.

[14] R.P. Bagwe, C. Yang, L.R. Hilliard, W. Tan, Langmuir 20 (2004) 8336-8342.

[15] L. Qian, X. Yang, Adv. Funct. Mater. 17 (2007) 1353-1358.

[16] W. Stöber, A. Fink, E. Bohn, J. Colloid Interface Sci. 26 (1968) 6269.

[17] B. Valeur, Molecular fluorescence: principles and applications. Wiley-VCH, Weinheim, 2001.

[18] G. Decher, J.D. Hong, J. Schmitt, Thin Solid Films 210-211 (1992) 831-835.

[19] A. van Blaaderen, A. Vrij, Langmuir 8 (1992) 2921-2931.

[20] C.A.R. Costa, C.A.P. Leite, F. Galembeck, J. Phys. Chem. B 107 (2003) 4747-4755.

[21] F. Bolletta, A. Juris, M. Maestri, D. Sandrini, Inorg. Chim. Acta 44 (1980) L175-L176.

[22] C.D. Borsarelli, S.E. Braslavsky, J. Phys. Chem. A 103 (1999) 1719-1727.

[23] M. Montalti, S.L. Murov, Handbook of photochemistry. CRC Press, Boca Raton, Fla., 2006.

[24] A. Slama-Schwok, D. Avnir, M. Ottolenghi, J. Am. Chem. Soc. 113 (1991) 3984-3985.

[25] P. Innocenzi, H. Kozuka, T. Yoko, J. Phys. Chem. B 101 (1997) 2285-2291.

[26] K. Osseo-Asare, F.J. Arriagada, Colloids Surf. 50 (1990) 321-339.

[27] K. Matsui, F. Momose, Chem. Mater. 9 (1997) 2588-2591.

[28] I. Fujita, H. Kobayashi, Inorg. Chem. 12 (1973) 2758-2762.

[29] F. Felix, J. Ferguson, H.U. Güdel, A. Ludi, J. Am. Chem. Soc. 102 (1980) 4096-4102.

[30] E. Krausz, Inorg. Chem. 27 (1988) 2392-2393.

[31] M.L. Bossi, M.E. Daraio, P. F. Aramendía, J. Photochem. Photobiol. A 120 (1999) 15-21.

[32] C.A.R. Costa, C.A.P. Leite, F. Galembeck, Langmuir 22 (2006) 7159-7166.

[33] A. Walcarius, C. Despas, J. Bessière, Microporous Mesoporous Mater. 23 (1998) 309-313.

[34] C. Despas, A. Walcarius, J. Bessière, Langmuir 15 (1999) 3186-3196.

[35] T.F. Tadros, J. Lyklema, J. Electroanal. Chem. 17 (1968) 267-275.

[36] H. Wright, R. Hunter, Aust. J. Chem. 26 (1973) 1191-1206.

[37] B.H. Milosavljevic, D. Meisel, J. Phys. Chem. B 108 (2004) 1827-1830.

Captions

Fig. 1. Sketch representation of the steps involved in the synthesis of $Ru(bpy)_3@SiO_2$ NPs.

Fig. 2. FE-SEM micrograph (A) and hydrodynamic size distribution (B) of $Ru(bpy)_3@SiO_2$ NPs.

Fig. 3. Emission spectra of $Ru(bpy)_3@SiO_2$ NPs dispersed in O_2-free and O_2-saturated water; λ_{exc} = 463 nm; slit = 0.5 mm.

Fig. 4. Quenching of the emission at 595 nm of $Ru(bpy)_3@SiO_2$ NPs by MV^{2+} as a function of pH (A) and MV^{2+} concentration (B); in A, [MV^{2+}] = 62 μM; in B, pH 3.0 (●), pH 8.9 (○).

Fig. 5. Emission spectra of $Ru(bpy)_3@SiO_2$ NPs (A), and emission at 595 nm (B) as a function of temperature; λ_{exc} = 463 nm; slit = 1.6 mm.

Fig. 6. Temperature response of the emission of $Ru(bpy)_3@SiO_2$ NPs after thermal cycling. The inset shows the decay of the maximum emission.

Fig. 7. 20 × 20 μm SCM images of $Ru(bpy)_3@SiO_2$ NPs adhered to PEI-modified glass (A), and mean fluorescence intensity as a function of temperature (B).

Fig. 8. 10 × 10 μm light transmission (A) and SCM (B) images of $Ru(bpy)_3@SiO_2$ NPs adhered to PEI-modified glass. (C) Intensity profiles of the spot marked with the arrow in A and B at 31.1 °C (●) and 38.4 °C (○); thick lines are Gaussian fits. (D) Particle fluorescence histogram for 31.1 °C (●) and 38.4 °C (○).

***3: Graphical Abstract (for review)**

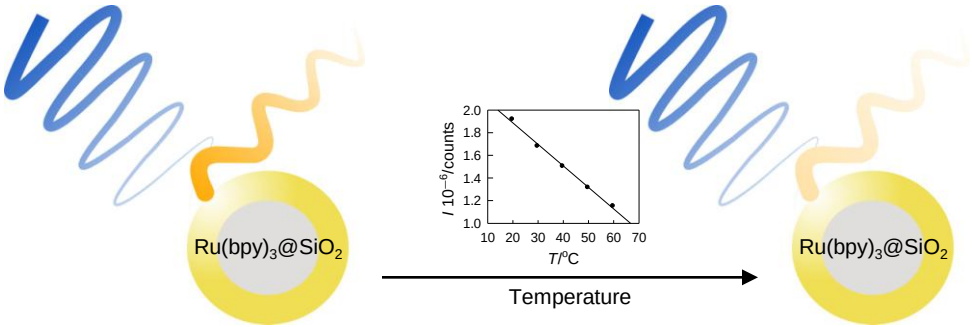

Highlights

- Colloidal tris(bipyridine)ruthenium(II)-doped silica nanoparticles are luminescent.
- Their emission decreases linearly with increasing temperature.
- Their phosphorescence is not affected by oxygen, nor negatively charged quenchers.
- They are suitable for sensing temperature in micro-environments.